Supplementary Materials for "Spatiotemporal Scattering and Interference at an Interluminal Interface between Synthetic Lattices"

Li Zhang[1, 2, 3, #], Rui Zhao[1, 3, #], Wenwen Liu[2, #], Kangpeng Ye[1], Junyao Wu[1, 3], Bei Wu[1, 3], Mingyu Tong[1, 3], Yuang Pan[1, 3], Fujia Chen[1, 3], Qiaolu Chen[1, 3], Yuze Hu[1, 3], Ning Han[4], Hongsheng Chen[1, 3, 5, 6], Lu Zhang[1, *], Yihao Yang[1, 3, 5, 6 *], and Shuang Zhang[2, 7, 8, 9, 10, *]

[1]State Key Laboratory of Extreme Photonics and Instrumentation, ZJU-Hangzhou Global Scientific and Technological Innovation Center, Zhejiang University, Hangzhou 310027, China.

[2]New Cornerstone Science Laboratory, Department of Physics, The University of Hong Kong, Hong Kong 999077, China.

[3]International Joint Innovation Center, The Electromagnetics Academy at Zhejiang University, Zhejiang University, Haining 314400, China.

[4]College of Optical and Electronic Technology, China Jiliang University, Hangzhou 310018, China

[5]Key Lab. of Advanced Micro/Nano Electronic Devices & Smart Systems of Zhejiang, Jinhua Institute of Zhejiang University, Zhejiang University, Jinhua 321099, China.

[6]Shaoxing Institute of Zhejiang University, Zhejiang University, Shaoxing 312000, China.

[7]State Key Laboratory of Optical Quantum Materials, University of Hong Kong, Hong Kong 999077, China.

[8]Quantum Science Center of Guangdong-Hong Kong-Macao Great Bay Area, 3 Binlang Road, Shenzhen 518000, China.

[9]Materials Innovation Institute for Life Sciences and Energy (MILES), HKU-SIRI, Shenzhen 518000, China.

[10]Department of Electrical & Electronic Engineering, The University of Hong Kong, Hong Kong 999077, China.

[#] These authors contributed equally

[*] Correspondence: *shuzhang@hku.hk* (S. Z.); *yangyihao@zju.edu.cn* (Y. Y.);
and *zhanglu1993@zju.edu.cn* (L. Z.).

Supplementary Note I. Experiment setup

As illustrated in Fig. S1a, our experimental setup comprises two fiber loops coupled via a variable beam splitter (VBS). The average round-trip propagation time within the system is approximately 24,620 ns, featuring a discrete time delay of 192 ns between the longer and shorter loops. A continuous wave at 1550 nm, emitted by a distributed feedback (DFB) laser, is injected into the system and shaped into a 60 ns pulse by an acousto-optic modulator (AOM). This pulse subsequently undergoes splitting and interference at the VBS. Within the shorter loop, a phase modulator (PM) and an intensity modulator (IM) precisely control the phase and amplitude of the circulating pulses to prepare the Gaussian-shaped wave packet. Propagation losses are compensated by erbium-doped fiber amplifiers (EDFAs). To suppress EDFA gain transients, a 1535 nm pilot laser is multiplexed with the signal. Then, both the pilot light and amplified spontaneous emission (ASE) noise are removed using band-pass filters (BPFs). Finally, a 50:50 beam splitter (BS) at the loop output couples a part of the signal to a photodetector (PD) for real-time capture and storage by a digital storage oscilloscope (DSO). The active components, including AOM, VBS, PM, and IM, are all driven by electrical signals from arbitrary waveform generators (AWGs). The rise time of these modulation signals is approximately 10 ns, which is significantly shorter than the average loop round-trip time, establishing a well-defined single period in the synthetic temporal lattice and successfully implementing a controlled moving interface.

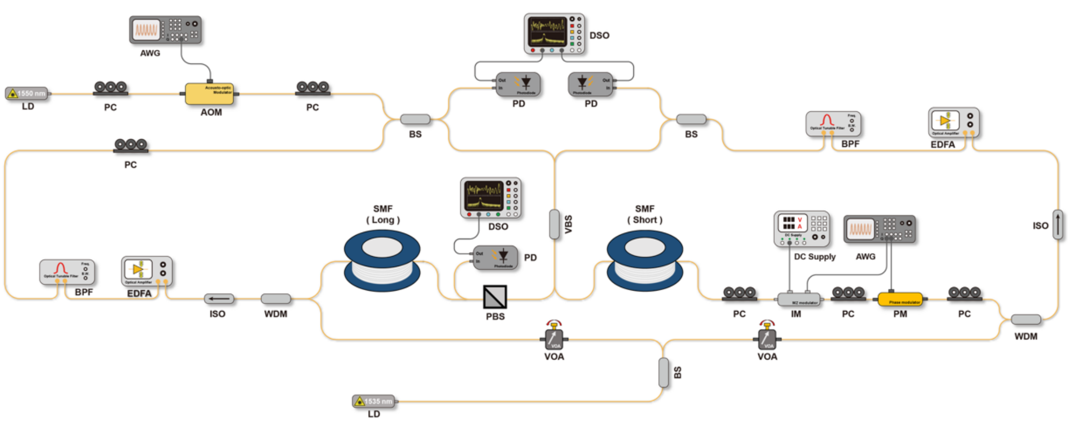

Fig. S1 Detailed experimental setup for construction of a moving spacetime interface in a synthetic temporal lattice. Sketch of experimental setup. LD: laser diode; AOM: acousto-optic modulator; BS: beam splitter; VBS: variable beam splitter; PBS: polarizing beam splitter; SMF:

single-mode fiber; WDM: wavelength division multiplexing coupler; ISO: isolator; EDFA: erbium-doped fiber amplifier; BPF: band-pass filter; PD: photodetector; VOA: variable optical attenuator; AWG: Arbitrary waveform generator; PC: polarization controller.

Supplementary Note II. Theoretical derivation of the band structure of the synthetic temporal lattice

To obtain the band structure of the Floquet synthetic temporal lattice, we start from the coupled evolution equations for a uniform lattice:

$$\begin{aligned} u_x^{t+1} &= \cos(\beta) u_{x+1}^t + i\sin(\beta) v_{x+1}^t \\ v_x^{t+1} &= i\sin(\beta) u_{x-1}^t + \cos(\beta) v_{x-1}^t \end{aligned}, \tag{1}$$

where u_x^t and v_x^t denote the pulse amplitudes in the short and long loops at lattice position x and time step t, respectively. Because the lattice exhibits discrete translation symmetry along both the spatial and temporal directions, the eigenstates take the Floquet-Bloch form

$$\begin{pmatrix} u_x^t \\ v_x^t \end{pmatrix} = e^{ikx - i\theta t} \begin{pmatrix} U \\ V \end{pmatrix}, \tag{2}$$

where k and θ denote the quasimomentum and quasienergy, respectively. Substituting this ansatz into Eq. (1) yields

$$e^{-i\theta} \begin{pmatrix} U \\ V \end{pmatrix} = \begin{pmatrix} \cos(\beta) e^{ik} & i\sin(\beta) e^{ik} \\ i\sin(\beta) e^{-ik} & \cos(\beta) e^{-ik} \end{pmatrix} \begin{pmatrix} U \\ V \end{pmatrix}. \tag{3}$$

Thus, the two-band Floquet dispersion can be written as,

$$\theta_{\pm}(k) = \pm\cos^{-1}(\cos(\beta)\cos(k)), \tag{4}$$

with $\theta_+(k)$ and $\theta_-(k)$ corresponding to the upper and lower bands.

Supplementary Note III. Generalized band-matching condition at a moving interface

The conservation law can be derived by transforming the ordinary coordinate frame to the oblique coordinate frame comoving with the interface. For an interface moving as $x = x_0 + v_{st}t$, we define the comoving coordinate

$$x' = x + v_{st} t. \tag{5}$$

The interface is stationary in this coordinate $x' = x_0$. A Floquet-Bloch mode in a homogeneous region has the phase

$$\varphi = kx - \theta t \,. \tag{6}$$

Using $x = x' + v_{st}t$, this phase becomes

$$\varphi' = kx' - \left(\theta - v_{st}k\right)t \,. \tag{7}$$

Thus, in the frame comoving with the interface, the effective quasienergy is

$$\theta' = \theta - v_{st}k \,. \tag{8}$$

Since the interface is stationary in the comoving coordinate, phase matching requires this comoving quasienergy to be conserved during scattering[1,2]:

$$\theta_{out} - vk_{out} = \theta_{in} - v_{st}k_{in} + 2\pi l \,. \tag{9}$$

Supplementary Note IV. Preparation of Gaussian incident wave packets

In the experiment, the Gaussian incident packet is prepared by independently programming the amplitudes and phases of the input pulse sequence[3,4]. The intensity modulation controls the amplitude of waves in the short loop, while the phase modulation imposes a phase across the pulse sequence. After a given number of preparation steps, the prepared field can be written as $E_n \sim \exp[-(n-n_0)^2/\Delta n^2]\exp(ik_i n)$, with a spatial width of Δn. Here, n labels the synthetic lattice site, n_0 is the packet center, and k_i is the central incident quasimomentum. When a Floquet band is targeted, the relative amplitudes and phases of the components are chosen to match the corresponding Bloch eigenvector. This experimentally generated pulse sequence, therefore, provides a finite-width approximation of the Floquet-Bloch wave packet used in the simulations and experiments. The preparation process of the Gaussian field distribution over 30-time steps is shown in Fig. S2.

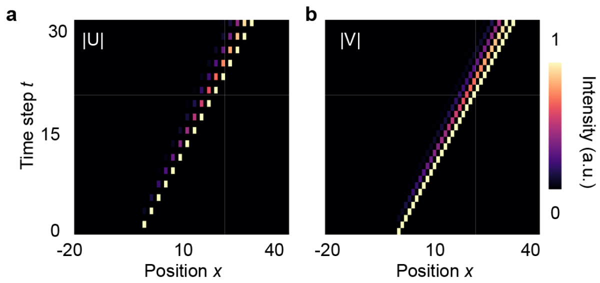

Fig. S2 Preparation of a Gaussian incident wave packet. a, b Simulated field evolutions in the short and long loops for the preparation of a Gaussian-shaped wave packet launched in the upper band with $k = 0.5\pi$ and $\beta = 0.39\pi$.

Supplementary Note V. Spatiotemporal scattering at interluminal interfaces for Gaussian incident packets with different widths

In this section, we perform numerical simulations using Gaussian incident wave packets with different spatial widths to investigate the influence of the finite wave-packet width on the scattering behavior. A broader Gaussian wave packet has a narrower momentum distribution and therefore provides a better approximation to a Floquet-Bloch state. Figure S3(a-d) shows the simulated field evolution for a Gaussian incident wave packet with $\Delta n = 10$. The scattering behavior is found to be similar to that obtained with a narrower incident wave packet, as shown in Figs. 3 and 4, indicating that the observed scattering effect is robust against the finite width of the input wave packet. To further quantify the scattering event, the transmission and reflection coefficients are calculated, as shown in Fig. S3(e-h). This confirms that the interluminal scattering features persist even when the incident Gaussian wave packet has a narrow bandwidth.

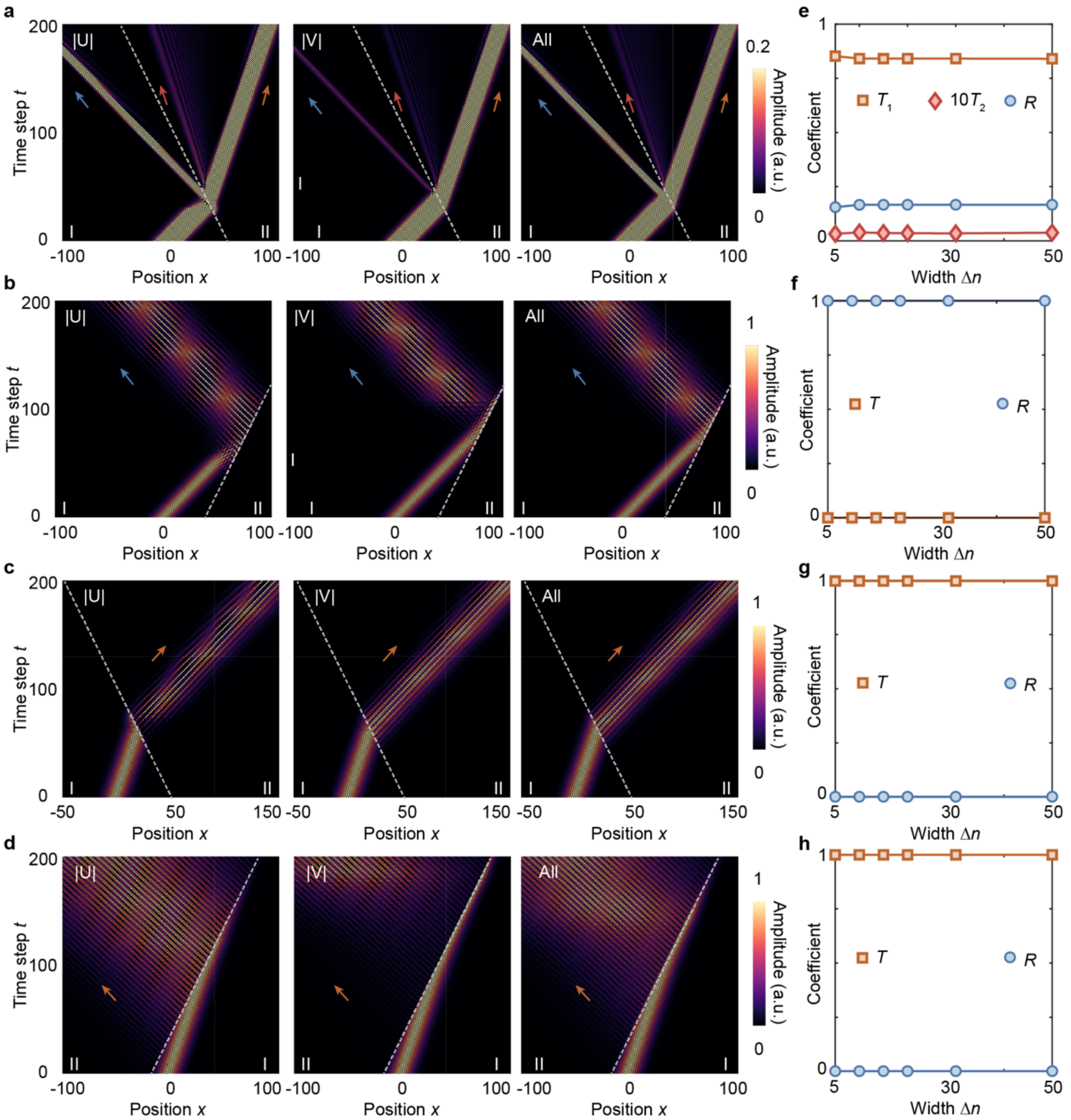

Fig. S3 Influence of the Gaussian wave-packet width on interluminal scattering. a-d Simulated field evolutions in the short, long loop and their combination for a Gaussian-shaped wave packet launched in the upper band with $k = 0.5\pi$. The grey dashed line represents the interluminal interface. The blue, red and orange arrows indicate the trajectories of the reflected and transmitted wave packets. **e-h** Calculated transmission and reflection coefficient versus the width of the Gaussian-shaped wave packet.

Supplementary Note VI. Scattering coefficients at an interluminal interface

In this section, we calculate the reflection and transmission efficiencies at the interluminal interface. The band-matching condition, together with the Floquet dispersion relation, determines all possible scattering channels. Real-valued roots correspond to propagating modes, whereas complex-valued roots correspond to evanescent modes. The outgoing reflected and transmitted channels are then selected according to their group velocities relative to the moving interface. Although evanescent modes do not carry energy away from the interface, they are required for a complete local matching of the wave function near the interface.

In the reference frame comoving with the interface, the wave function of a mode can be written as

$$\psi(x',t)=\begin{bmatrix}U(x',t)\\V(x',t)\end{bmatrix}=\begin{bmatrix}U'(x')\\V'(x')\end{bmatrix}e^{-i\theta' t}. \tag{10}$$

The total wave function is then expanded as a superposition of the incident mode, all outgoing reflected and transmitted modes, and the evanescent modes. On the incident side,

$$\psi_L(x')=\psi_{in}(x')+\sum_j r_j\psi_{L,j}^{out}(x')+\sum_n r_{e,n}\psi_{L,n}^{eva}(x'). \tag{11}$$

On the transmitted side,

$$\psi_R(x')=\sum_j t_j\psi_{R,j}^{out}(x')+\sum_n t_{e,n}\psi_{R,n}^{eva}(x'). \tag{12}$$

Here, r_j and t_j are the reflection and transmission amplitudes of the propagating modes, while $r_{e,n}$ and $t_{e,n}$ are the reflection and transmission amplitudes of evanescent modes. The coefficients are obtained by substituting this total wave function expansion into the discrete evolution equations in the comoving frame. The boundary condition is not imposed as a simple continuity condition at a single point. Instead, the total wave function should satisfy the lattice evolution at every step that crosses the interface[2].

For an interface located at $x'=x_0$, the coupling parameters are different on the two sides. Therefore, only those equations whose input and output positions lie on different sides of the interface give nontrivial matching equations. In the comoving frame, the U'-component at position x' couples $U'(x')$ to the input fields at $x'+1+v_{st}$. Thus, this equation crosses the interface when

$$\min(x',x'+1+v_{st})\le x_0\le\max(x',x'+1+v_{st}). \tag{13}$$

Similarly, the V'-component at position x' couples $V'(x')$ to the input fields at $x'-1+v_{st}$. This equation crosses the interface when

$$\min(x',x'-1+v_{st})\le x_0\le\max(x',x'-1+v_{st}). \tag{14}$$

At all such positions, the total wavefunction expansion is substituted into the corresponding discrete equation, which gives a finite linear system,

$$\mathbf{M}\begin{pmatrix} r_1 & r_2 & \dots & t_1 & t_2 & \dots & r_{e,1} & r_{e,2} & \dots & t_{e,1} & t_{e,2} & \dots \end{pmatrix}^T = \mathbf{b}. \quad (15)$$

Here, **b** is determined by the incident mode and **M** is determined by the interface profile and the Floquet-Bloch eigenmodes. Solving this linear system gives the reflection and transmission amplitudes. The scattering efficiencies can be obtained by normalizing the outgoing fluxes to the incident flux. For the case with $v = -1/2$ shown in Fig. 3b, we obtain $R = 0.17$, $T_1 = 0.83$ and $T_2 = 0.004$, in good agreement with the calculated results shown in Fig. S3e.

Supplementary Note VII. Effective interference in the interluminal slab

In this section, we present a minimal model for the effective interference of internal propagating channels in the interluminal slab, which result in the width-controlled order selection. Before the nth encounter with the second interface, the field in the slab can be written as a superposition of accessible propagating channels in region II,

$$\psi_n^{in}(L) = \sum_j a_{n,j}(L)\psi_j^{\mathrm{II}}. \quad (16)$$

Here, $a_{n,j}(L)$ is the amplitude of the jth propagating channel, and ψ_j^{II} denotes its wave function in region II. Both the magnitude and phase of $a_{n,j}(L)$ are determined by the previous propagation and scattering inside the slab. Thus, changing the slab width L modifies the complex amplitudes of the propagating channels when they reach the second interface.

When these channels scatter at the second interface, each channel contributes to the mth outgoing channel in region III with a channel-dependent complex transmission amplitude $t_{j,m}^{out}$. Therefore, the output field after the nth encounter in region III can be written as

$$\psi_n^{out}(L) = \sum_m A_{n,m}^{out}(L)\psi_m^{\mathrm{III}}, \quad (17)$$

where $A_{n,m}^{out}(L)$ is the amplitude of the mth outgoing channel, given by

$$A_{n,m}^{out}(L)=\sum_j t_{j,m}^{out}a_{n,j}(L). \tag{18}$$

The successive leakage events can be described by a minimal effective feedback model, where we assume there can only exists one outgoing channel in region III. We consider $\mathbf{a}_1 = (a_{1,1}, a_{1,2}, a_{1,3}, \ldots)^T$ as the internal channel amplitudes before the first encounter with the second interface, and $\mathbf{t}=\left(t_1^{out},t_2^{out},t_3^{out}\ldots\right)$ as the complex transmission amplitudes from the internal channels to the outgoing channel. The first leakage amplitude can be written as,

$$A_1^{out}=\mathbf{ta}_1. \tag{19}$$

The remaining field is then reflected into the slab and undergoes one feedback cycle, represented by an effective matrix $\boldsymbol{R}(L)$. In this way, the second and third leakage amplitudes can be written as,

$$A_2^{out}=\mathbf{tR}(L)\mathbf{a}_1, \tag{20}$$

$$A_3^{out}=\mathbf{tR}^2(L)\mathbf{a}_1. \tag{21}$$

These expressions show that the relative strength of transmitted order is governed by the effective interference of internal propagating channels at the second interface. Changing L modifies their accumulated phases during propagation and feedback, thereby changing scattering-weighted amplitudes A_n^{out}. As a result, the leakage can be enhanced at the first encounter or delayed to the next feedback cycle, producing the observed oscillatory variation between first- and second-order-dominant transmission. Although higher-order leakage events can in principle occur, each additional order requires another feedback cycle and is progressively reduced by partial leakage, channel redistribution and wave-packet spreading, resulting in weak higher transmitted orders in the present configuration.

Supplementary Note VIII. Spatiotemporal scattering in other interluminal slabs

In this section, we further study two additional interluminal slab configurations beyond the geometry discussed in Fig. 5, which illustrate how different combinations of interluminal interfaces give rise to distinct scattering pathways. First, we consider a contradirectional slab in which regions I and III share the same coupling angle β_1 = 0.08π, whereas the central slab region is set to β_2 = 0.39π. As shown in Fig. S4a, a Gaussian-wave packet in the upper band with initial quasimomentum k = 0.5π is launched towards the slab. At the first interface, the incident packet produces one reflected and two transmitted wave packets according to the band-matching condition. The dominant transmitted branch then reaches the second interface, where it is converted into an outgoing transmitted wave without further reflection. Consequently, the slab produces a finite output consisting of a single reflected component and finite transmitted components.

When the coupling angles are interchanged (central slab β = 0.08π, side regions β = 0.39π), the scattering dynamics change dramatically (Fig. S4b). In this case, the first interface is reflectionless, and the incident pulse is injected completely into the slab. At the second interface, however, the wave undergoes channel splitting into reflected and transmitted components. The reflected part then propagates back to the first interface, where it is totally reflected and sent back into the slab. This process establishes a recurrent feedback loop between the two interfaces, similar to that in Fig. 5.

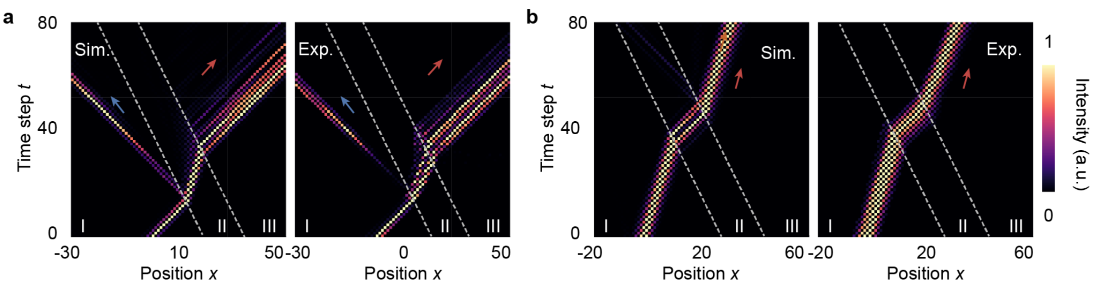

Fig. S4 Spatiotemporal scattering in interluminal slabs. a, b Simulated and experimentally measured field evolutions for interluminal slabs. The grey dashed line represents the interluminal interface. The blue and red arrows indicate the trajectories of the reflected and transmitted wave packets.

Reference

1. Y. Yu, H. Hu, L. Zou *et al.* Antireflection Spatiotemporal Metamaterials. ***Laser & Photon. Rev.*** 17, 2300130 (2023).
2. C. Qin, H. Ye, S. Wang *et al.* Observation of discrete-light temporal refraction by moving potentials with broken Galilean invariance. ***Nat. Commun.*** 15, 5444 (2024).
3. A. Regensburger, C. Bersch, M. A. Miri *et al.* Parity-time synthetic photonic lattices. ***Nature*** 488, 167-171 (2012).

4. M. Wimmer, A. Regensburger, C. Bersch *et al.* Optical diametric drive acceleration through action–reaction symmetry breaking. ***Nat. Phys.*** 9, 780-784 (2013).